Isothermal Desorption Kinetics of Crystalline H_2O, $H_2{}^{18}O$, and D_2O Ice Multilayers

Jamison A. Smith,[†] Frank E. Livingston,[‡] and Steven M. George*[,§]

Department of Chemistry and Biochemistry, University of Colorado, Boulder, Colorado 80309-0215

Received: November 27, 2002; In Final Form: February 6, 2003

The isothermal desorption rates of crystalline H_2O, $H_2{}^{18}O$, and D_2O ice multilayers were measured over a temperature range from 175 to 190 K. The desorption rates were measured with optical interferometry using ice multilayers grown epitaxially on a Ru(001) surface in an ultrahigh vacuum chamber. The Arrhenius parameters for the desorption of H_2O and $H_2{}^{18}O$ were identical within experimental error. For H_2O, the preexponential was $\nu = 10^{32.6\pm0.3}$ cm^{-2} s^{-1} and the activation energy was $E = 13.9 \pm 0.2$ kcal mol^{-1}. For $H_2{}^{18}O$, the preexponential was $\nu_{18} = 10^{32.4\pm0.3}$ cm^{-2} s^{-1} and the activation energy was $E_{18} = 13.8 \pm 0.2$ kcal mol^{-1}. Despite the near equivalence in the Arrhenius parameters, $H_2{}^{18}O$ desorbed at a rate that was slower by ~9% throughout the range of temperatures. In contrast, the desorption rate of D_2O was slower by 49−62% compared with H_2O over the measured temperature range. The Arrhenius parameters for the desorption of D_2O were $\nu_D = 10^{33.4\pm0.5}$ cm^{-2} s^{-1} and $E_D = 14.8 \pm 0.4$ kcal mol^{-1}. A transition state model was developed to explain the measured desorption kinetics. The transition state model predicts that total molecular mass has only a small effect on the desorption kinetics because the mass differences among the isotopomers are small. On the other hand, the principal moments of inertia of the desorbing molecules have a large effect on the desorption rate. About each of the three axes, D_2O has roughly twice the moment of inertia of H_2O or $H_2{}^{18}O$. This larger moment of inertia affects the desorption rate in two ways. First, surface bound D_2O molecules have lower frequencies for hindered rotations. These lower frequencies result in less zero-point energy for the surface bound molecule and a larger desorption activation energy. Second, a transition state D_2O molecule has a larger rotational partition function. This larger rotational partition function yields a larger preexponential for desorption.

I. Introduction

Isotopes are valuable in understanding physical processes. In the Earth's atmosphere, the heavy isotopomers of water are condensed preferentially because they have a lower equilibrium vapor pressure than does H_2O. Many studies have measured fractionation factors[1−6] and equilibrium vapor pressures[7−16] of the various isotopomers. The effect of isotope on vapor pressure has been summarized for water and ice.[9] The preferential condensation of heavy isotopomers is temperature dependent. Consequently, the isotopic composition of ice cores can be used in conjunction with other techniques as a paleothermometer.[17,18]

H_2O isotopomers have been employed previously to study the kinetics of self-diffusion in ice.[19−24] These laser-induced thermal desorption (LITD) experiments have revealed that the diffusion kinetics for HDO and $H_2{}^{18}O$ are very similar. HDO displayed a diffusion activation barrier of $E_A = 17.0 \pm 1.0$ kcal mol^{-1} and a diffusion preexponential of $D_0 = (4.2 \pm 0.8) \times 10^8$ cm^2 s^{-1}.[20,22] Comparison with the desorption kinetics revealed that HDO and $H_2{}^{18}O$ isotopomers adsorbed on an ice surface can diffuse into the ice bulk on a time scale that is comparable to the time scale for desorption into vacuum.

The isotope effect on the kinetics of ice desorption has not been examined completely. The desorption rate of H_2O ice has been measured in many studies.[19,21,25−28] Desorption kinetics have been reported for D_2O ice.[28,29] However, no desorption kinetics have been reported for $H_2{}^{18}O$ ice. To provide a complete comparison, the desorption rate of crystalline ice was measured with optical interferometry on samples made from the three isotopomers: H_2O, $H_2{}^{18}O$, and D_2O.

This study revealed that the desorption kinetics of $H_2{}^{18}O$ are very similar to the desorption kinetics of H_2O. In contrast, D_2O exhibits very different desorption kinetics. The differences among the H_2O isotopomers are explained using a transition state model. The similarities and differences among the isotopomers were justified by the rotational degrees of freedom and the moments of inertia of the H_2O isotopomers. D_2O has a lower frequency of hindered rotation on the ice surface that leads to less zero-point energy and a larger desorption energy. D_2O also has a larger rotational partition function at the transition state that leads to a larger desorption preexponential.

II. Experimental Section

The desorption experiments were performed in an ultrahigh vacuum chamber that has been described previously.[30] Briefly, the chamber is pumped by a 200 L s^{-1} ion pump and titanium sublimation pump. The base pressure of the chamber before experimentation was less than 1×10^{-9} Torr as measured by a nude Alpert-Bayard ion gauge. The residual gas observed with a quadrupole mass spectrometer was primarily the various H_2O isotopomers.

The ice films were grown by vapor deposition onto a single-crystal Ru(001) substrate. The $\sqrt{3} \times \sqrt{3}$ R30° unit cell on the

* Corresponding author.
[†] Present Address: Laboratory for Atmospheric and Space Physics, University of Colorado, Boulder, CO 80309-0392.
[‡] Present Address: Aerospace Corporation, 2350 E. El Segundo Blvd., El Segundo, CA 90245-4691.
[§] Presently jointly appointed with the Department of Chemical Engineering, University of Colorado, Boulder, CO 80309-0424.

10.1021/jp022503s CCC: $25.00
Published on Web 04/01/2003

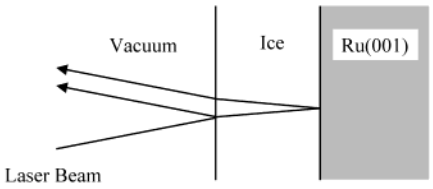

Figure 1. Schematic of the optical interferometry experiment.

Ru(001) surface has an excellent lattice match with hexagonal ice.[31] The water vapor was drawn from glass bulbs containing the various liquid water isotopomers. Prior to deposition, the liquid water was degassed by a freeze, pump, and thaw procedure. The sources of liquid water isotopomers were H_2O (HPLC grade, Aldrich), $H_2{}^{18}O$ (97+% ^{18}O, Cambridge Isotopes), and D_2O (99.996% D, Cambridge Isotopes).

The temperature of the ruthenium substrate was maintained by simultaneously cooling and heating. Cooling was provided by a cryostat filled with liquid nitrogen.[32] Two tantalum foils (0.010 in. thick) served as resistive heating elements. These foils were spot-welded to the back of the ruthenium substrate and clamped to the cryostat. The resistive heating was controlled with a laboratory-built temperature controller. The temperature was measured with a pair of tungsten−rhenium (W−5%Re/W−26%Re) thermocouple wires (0.003 in. diam) that were spot-welded to the back of the ruthenium substrate. The stability of the temperature during a desorption experiment was ±0.2 K. The precision of the temperature measurements among all the experiments in this study was ±0.1 K. The accuracy of the absolute temperature measurement is ±2 K.

The ice films were prepared by dosing the Ru(001) substrate with a collimated source of water molecules. Leak valves (MD-7, Vacuum Generators) were used to provide a controlled leak of water vapor through the glass capillary array dosers (C13S10M50, Galileo). These capillary array dosers produced a local H_2O pressure over the Ru(001) substrate that was ∼200 times higher than the pressure in the chamber. Film growth was performed by exposing the substrate to an effective H_2O pressure of 7×10^{-5} Torr for 180 s. This procedure produced ice films with a thickness of 6 μm. The temperature of the substrate was maintained at 160 K during film growth. A previous study has shown that ice deposited from the vapor onto Ru(001) is crystalline when deposited at 160 K.[19]

The isothermal desorption rate of the ice films was measured using optical interferometry.[26,27] A nonpolarized helium−neon laser with a wavelength of 594 nm (Melles Griot, model 05-LYR-173) was employed for these optical interferometry studies. The laser beam entered the vacuum chamber through a $4^1/_2$-in. sapphire viewport. The reflected beam exited the chamber through the same viewport. The angle of incidence of the laser beam was ∼5° from the normal of the Ru(001) surface. The intensity of the recombined beam was measured with a photodiode (FOD-100, EG&G) operated in a reverse bias configuration. A schematic of the optical geometry in the interference experiment is shown in Figure 1.

The intensity of the reflected beam depends on the phase difference between the two recombining beams. This phase difference depends on the difference in path length between the recombining beams. The phase, β, acquired by a beam travelling a distance, z, through an ice film is given by

$$\beta = \frac{2\pi n z}{\lambda} \tag{1}$$

where n is the index of refraction of the ice, and λ is the wavelength of light in a vacuum. If the angle of incidence is near-normal and z is the thickness of the ice film, then the beam transmitted at the vacuum/ice interface must travel an extra distance of $2z$ before recombining with the beam reflected from the vacuum/ice interface. As a result, the phase difference, $\Delta\beta$, acquired from the difference in path length is 2β.

During isothermal desorption, the phase difference changes with decreasing film thickness. The desorption kinetics of ice multilayers are zero order.[33] Consequently, the ice film thickness decreases linearly with time during isothermal desorption. The phase difference and the reflectivity change with decreasing film thickness. As the reflectivity passes from one minimum to another, the phase difference changes by 2π. The difference in ice thickness corresponding to adjacent minima in the reflectivity, Δz, is

$$\Delta z = \frac{\lambda}{2n} \tag{2}$$

where Δz corresponds to 227 nm, i.e., the desorption of 618 bilayers of ice at the temperatures of the desorption experiments.

The rate of change of the film thickness, dz/dt, is then determined from Δz and the frequency, ν, of the reflectivity signal:

$$\frac{dz}{dt} = \nu \Delta z \tag{3}$$

The H_2O desorption rate from the ice film, ϕ, can be calculated from the number density of H_2O molecules in the ice lattice, N, and the rate of change of the film thickness:

$$\phi = N\frac{dz}{dt} \tag{4}$$

Substituting eqs 2 and 3 into eq 4 yields

$$\phi = N\frac{\lambda}{2n}\nu \tag{5}$$

The lattice constants for H_2O and D_2O ice have been measured over a wide range of temperatures.[34] The variation in the lattice constants of a particular isotopomer over the temperature range of this study is <0.1%. Variation between the lattice constants of H_2O and D_2O at a given temperature is <0.1%. As a result, a mean number density of 3.10×10^{22} cm^{-3} was employed for all the H_2O isotopomers.

The refractive index for ice was assumed to be independent of temperature and isotope. Calculations of the refractive index from previously available experimental data show that the refractive index of crystalline ice is independent of temperature in the visible region of the electromagnetic spectrum.[35] In agreement with the refractive index calculations, independent measurements of the refractive index at $\lambda = 633$ nm showed that $n = 1.31$ for vapor-deposited ice when the deposition temperature was greater than 140 K.[36] Variation of the refractive index with respect to isotope is unknown but expected to be negligible because of the similarity in lattice constants and electronic structure for the isotopomers.

III. Results

Figure 2 compares the optical interferometry traces for the desorption of H_2O, $H_2{}^{18}O$, and D_2O ice films at a low temperature of 175 K. The various reflectivities have been vertically displaced for clarity in presentation. The oscillations in the reflectivity are clearly visible. The oscillation amplitude was ∼9% of the average reflectivity. The oscillation frequencies

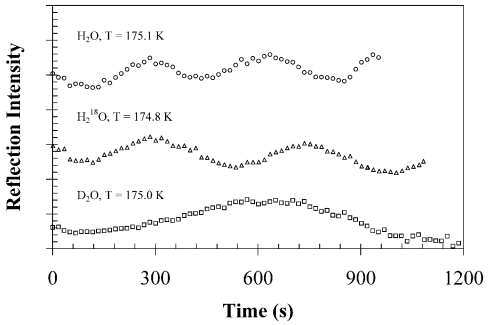

Figure 2. Optical interferometry signals versus time during isothermal desorption at 175 K. The traces have been displaced vertically for clarity.

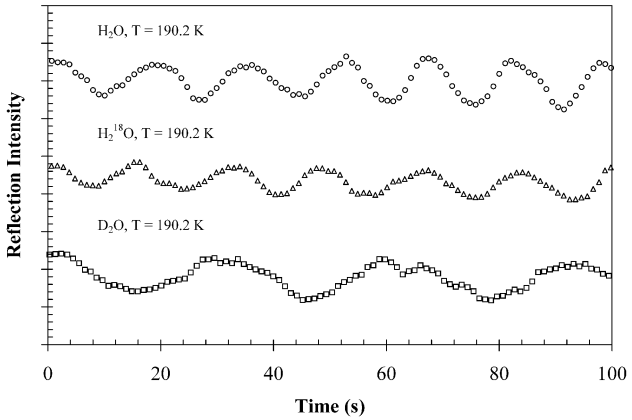

Figure 3. Optical interferometry signals versus time during isothermal desorption at 190 K. The traces have been displaced vertically for clarity.

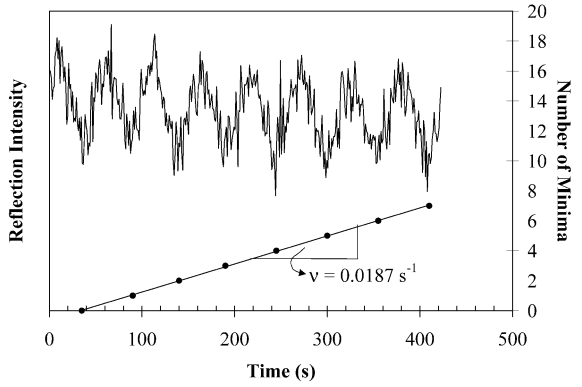

Figure 4. Calculation of the reflectivity frequency for an H_2O multilayer desorbing at 184 K.

for H_2O and $H_2{}^{18}O$ are similar. The oscillation frequency for D_2O is roughly half that of H_2O.

Figure 3 compares the optical interferometry traces for the desorption of H_2O, $H_2{}^{18}O$, and D_2O ice films at a high temperature of 190 K. The different traces have again been vertically displaced for clarity in presentation. Like the results at 175 K, the oscillation frequencies for H_2O and $H_2{}^{18}O$ are similar. The oscillation frequency for D_2O is roughly half that of H_2O.

Optical interferometry signals were recorded during isothermal desorption experiments at temperatures between 175 and 195 K. Figure 4 shows the reflectivity during isothermal desorption of an H_2O ice film at a temperature of 184 K. The frequency of the reflectivity signal was calculated from a linear fit of the number of minima versus time. The reflectivity

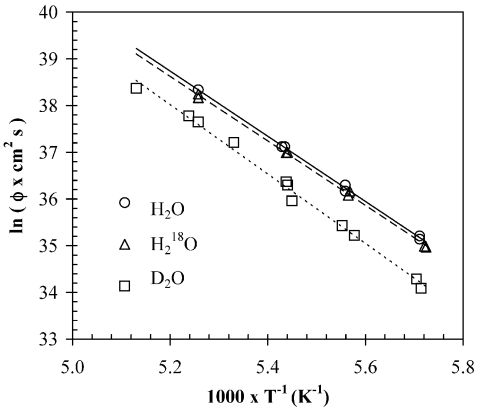

Figure 5. Arrhenius plot of the observed desorption rates for H_2O, $H_2{}^{18}O$, and D_2O ice multilayers. The lines are linear fits to the data.

TABLE 1: Arrhenius Parameters for the Desorption of H_2O Isotopomers from Ice Multilayers (Preexponentials are in units of cm^{-2} s^{-1}, and the activation energies are in units of kcal mol^{-1})

isotopomer	preexponential	activation energy
H_2O	$10^{32.6\pm0.3}$	13.9 ± 0.2
$H_2{}^{18}O$	$10^{32.4\pm0.3}$	13.8 ± 0.2
D_2O	$10^{33.4\pm0.5}$	14.8 ± 0.4

TABLE 2: Comparison of Isotopomer Mass, Experimental Desorption Rate at 183.9 ± 0.02 K and Moment of Inertia about the *c*-Axis (Masses are in units of amu, desorption rates are in units of cm^{-2} s^{-1}, and moments of inertia are in units of amu $Å^2$)

isotopomer	mass	desorption rate	moment of inertia
H_2O	18	$(1.32 \pm 0.01) \times 10^{16}$	2
$H_2{}^{18}O$	20	$(1.17 \pm 0.01) \times 10^{16}$	2
D_2O	20	$(0.60 \pm 0.03) \times 10^{16}$	4

frequencies for all of the isothermal experiments were calculated in this manner. The reflectivity frequency for each experiment was then used to calculate the observed desorption rate.

Figure 5 displays an Arrhenius plot of the observed desorption rates from the ice multilayers. The desorption kinetics of H_2O and $H_2{}^{18}O$ are almost identical except that the desorption rate for $H_2{}^{18}O$ is slower by ~9%. The desorption kinetics of D_2O are much slower and markedly distinct from the desorption kinetics of H_2O and $H_2{}^{18}O$. The Arrhenius parameters extracted from a linear regression of the data in Figure 5 are listed in Table 1. The stated uncertainty is the standard error in determining the slope and intercept from the linear regression.

IV. Discussion

The desorption kinetic parameters of H_2O and $H_2{}^{18}O$ are very similar. The activation energies of 13.9 ± 0.2 kcal mol^{-1} and 13.8 ± 0.2 kcal mol^{-1} for H_2O and $H_2{}^{18}O$ desorption are identical within experimental error. The preexponentials of $10^{32.6\pm0.3}$ molecules cm^{-2} s^{-1} and $10^{32.4\pm0.3}$ molecules cm^{-2} s^{-1}, for H_2O and $H_2{}^{18}O$ desorption, respectively, are also equivalent within experimental error. In contrast, the desorption parameters for D_2O are different. D_2O displays a larger activation energy of 14.8 ± 0.4 kcal mol^{-1} and a larger desorption preexponential of $10^{33.4\pm0.5}$ molecules cm^{-2} s^{-1}.

The desorption kinetics of an H_2O isotopomer from an ice surface are correlated more with the principal moments of inertia of the desorbing molecule than with the mass. To illustrate this correlation, Table 2 lists the mass, the experimental desorption rates at 183.9 ± 0.2 K, and the moment of inertia about the *c*-axis for each isotopomer. D_2O is distinct from H_2O and $H_2{}^{18}O$

TABLE 3: Observed Physical Constants of H_2O Isotopomers in Units of cm^{-1}[a]

			H_2O	$H_2{}^{18}O$	D_2O
gas	ν_1		3657.05 [43]	3649.68 [42]	2671.46 [41]
	ν_2		1594.59 [41]	1588.275 [44]	1178.33 [41]
	ν_3		3755.97 [43]	3741.58 [42]	2688.05 [41]
	A_0		27.8806 [45]	27.5312 [45]	15.3846 [41]
	B_0		14.5216 [45]	14.5218 [45]	7.2716 [41]
	C_0		9.27770 [45]	9.23802 [45]	4.8458 [41]
surface	ν_1	dH/D	3693 [47]	n/a	2726 [47]
		dO	3560 [47]	n/a	2640 [47]
		s4	3440 [47]	n/a	2530 [47]
	ν_2	dH/D	1652 [47]	n/a	1213 [46]
		dO	1684 [47]	n/a	1230 [46]
		s4	1702 [47]	n/a	1244 [46]
	ν_3	dH/D	3100 [47]	n/a	2300 [46]
		dO	3330 [47]	n/a	2480 [46]
		s4	3240 [47]	n/a	2435 [46]
	ν_R		n/a	n/a	n/a
	ν_T		n/a	n/a	n/a
bulk	ν_R		840 [48]	n/a	640 [48]
	ν_T		229.2 [49]	n/a	221.7 [49]

[a] n/a = not available.

in that D_2O has twice the moment of inertia about all three principal axes. These large differences in moment of inertia are responsible for the markedly slower desorption kinetics of D_2O.

As will be shown by the transition state model developed below, the larger moment of inertia of D_2O results in a lower frequency of hindered rotation on the ice surface. The lower frequency of hindered rotation results in less energy stored in zero-point motions and a larger activation energy for desorption. At the transition state, the larger moment of inertia of D_2O results in a larger rotational partition function and a larger preexponential for desorption.

A. Transition State Model. Transition state theory was employed to understand the absolute desorption rate of H_2O ice and to explain the isotope effect. This development is similar to an earlier transition state model[37] and a previous review of the vapor pressure isotope effect.[9] The reactant in this model is a surface-bound H_2O, $H_2{}^{18}O$, or D_2O molecule. The transition state is a desorbing H_2O, $H_2{}^{18}O$, or D_2O molecule that is moving away from the ice surface. The transition state is far enough from the ice surface that the desorbing molecule is nearly free.

The transition state expression for the desorption rate is

$$\phi_d = \theta \frac{k_B T}{h} \frac{Q^*}{Q_s} \exp\left(\frac{-E_0}{k_B T}\right) \tag{6}$$

where θ is the concentration of surface bound molecules, Q^* is the transition state partition function with the desorption coordinate removed, Q_s is the surface bound partition function, and E_0 is the energy difference between the zero-point of the surface bound molecule and the zero-point of the transition state. The concentration of surface bound H_2O molecules is not well-known. The basal facet of hexagonal ice, $I_h(0001)$, has a surface concentration of 1.14×10^{15} molecules cm^{-2} as calculated from the ideal tetrahedral structure of I_h and measured lattice parameters.[34] The ice surface is believed to be disordered at these temperatures with surface molecules bound to non-crystallographic sites via strained hydrogen bonds.[38−40] Consequently, a surface concentration of 1.0×10^{15} cm^{-2} is used as an estimate.

The partition function of the transition state was constructed from three intramolecular vibrations, three free rotations, and two free translations. The third free translation is the desorption coordinate. The partition function for the three intramolecular vibrations is

$$q_v^* = \prod_{i=1}^{3} \left(\frac{1}{1 - e^{-(h\nu_i/k_B T)}} \right) \tag{7}$$

The frequencies of the three vibrations have been measured for gas-phase H_2O, $H_2{}^{18}O$, and D_2O.[41−44] These frequencies are listed in Table 3.

The partition function for the free rotations is

$$q_r^* = \frac{\sqrt{\pi}}{2} \sqrt{\frac{T^3}{\theta_A \theta_B \theta_C}} \tag{8}$$

The 2 is a symmetry factor to account for the indistinguishibility of the hydrogens in the three isotopomers. θ_i is the rotational temperature of the molecule about each of its principal axes:

$$\theta_A = \frac{hcA_0}{k_B} \tag{9}$$

where A_0 is the rotational constant for the *a*-axis. Analogous expressions are used for θ_B and θ_C. The rotational constants have been measured and are listed in Table 3.[41,45]

The partition function for free two-dimensional translation is

$$q_t^* = \frac{2\pi m k_B T}{h^2} A \tag{10}$$

The area of the transition state, *A*, is not well-known. This 2-D box of unknown area is portrayed in Figure 6. The area of this 2-D box was tuned in conjunction with the classical desorption energy, E_c, to match the observed desorption kinetics for H_2O.

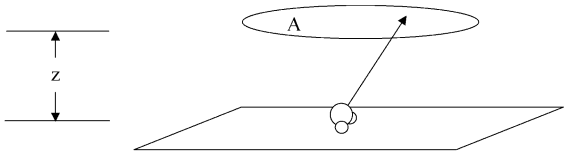

Figure 6. The area, *A*, of the 2-D translational box for the transition state. *z* is the distance between the transition state and the surface and $A \sim \pi z^2$. *A* is a free parameter that is tuned to achieve agreement between the theoretical and experimental desorption rates for H_2O multilayers.

The partition function for the surface molecule was constructed from three intramolecular vibrations, three hindered rotations, and three hindered translations. The intramolecular vibrations of H_2O and D_2O molecules on an ice surface have been measured experimentally and are listed Table 3.[46,47] The center of the vibrational peaks depends on the orientation and degree of hydrogen bonding to the ice surface, e.g. dangling H or D (dH/D), dangling O (dO), or strained tetrahedral (s4). The frequencies used in this treatment are the arithmetic mean of the frequencies for the different observed configurations. The values for $H_2{}^{18}O$ were estimated from the values for H_2O and the ratio of the gas-phase frequencies between the two isotopomers. Consequently, the frequency of an intramolecular vibration for an $H_2{}^{18}O$ molecule on the surface was estimated to be

$$\nu_{18,s,i} = \nu_{16,s,i} \frac{\nu_{18,g,i}}{\nu_{16,g,i}} \tag{11}$$

TABLE 4: Physical Constants Used to Calculate the Partition Functions for H_2O Isotopomers in Units of cm^{-1}

		H_2O	$H_2{}^{18}O$	D_2O
transition state	ν_1	3657	3650	2671
	ν_2	1595	1588	1178
	ν_3	3755	3742	2688
	A_0	27.88	27.53	15.38
	B_0	14.52	14.52	7.272
	C_0	9.278	9.238	4.846
surface	ν_1	3564	3557	2632
	ν_2	1679	1673	1229
	ν_3	3223	3211	2405
	ν_R	727.5	725.1	554.3
	ν_T	198.5	188.3	192.0

The vibrational frequencies used to determine the partition functions are listed in Table 4.

Bulk H_2O and D_2O ice rotational bands have been measured and are listed in Table 3.[48,49] These frequencies were modified by $\sqrt{3/4}$ to account for looser binding at the surface, i.e., the average bulk molecule shares 4 hydrogen bonds and the average surface molecule shares 3 hydrogen bonds. The value for $H_2{}^{18}O$ was estimated from the value for H_2O and the gas-phase rotational constants. The frequency of a hindered rotation is proportional to the reciprocal of the square root of the moment of inertia, $\nu \alpha \sqrt{I}^{-1}$. The moment of inertia about a principal axis is proportional to the reciprocal of the rotational constant, $I_A \alpha A_0^{-1}$. Consequently, the frequency of a hindered rotation for $H_2{}^{18}O$ on the surface was estimated to be proportional to the square root of the rotational constant, $\nu_A \alpha \sqrt{A_0}$. The three rotations are represented by a mean frequency. The mean rotational frequency is obtained by averaging the square roots of the rotational constants:

$$\nu_{18,s,rot} = \frac{\sum_{i=A}^{C}\sqrt{i_{0,18}}}{3}\frac{\nu_{16,s,rot}}{\frac{\sum_{i=A}^{C}\sqrt{i_{0,16}}}{3}} \qquad (12)$$

The rotational frequencies used to determine the partition functions are listed in Table 4.

Bulk H_2O and D_2O ice translational bands have been measured and are listed in Table 3.[48,49] These frequencies were modified by $\sqrt{3/4}$ to account for looser binding at the surface. The frequency of a hindered translation should be proportional to the reciprocal of the square root of the total molecular mass, $\nu \alpha \sqrt{m}^{-1}$. For $H_2{}^{18}O$, the hindered translation frequency was estimated by multiplying the frequency of H_2O by $\sqrt{18/20}$. The translational frequencies used to determine the partition functions are listed in Table 4.

Calculating the desorption rate with the transition state expression requires the difference in energy between the zero-point of the surface molecule and the zero-point of the transition state as depicted in Figure 7. The zero-point contributions from each oscillator, i.e. the intramolecular vibrations and the hindered intermolecular motions, are calculated from estimated vibrational frequencies as

$$ZP_i = \frac{1}{2}h\nu_i \qquad (13)$$

These frequencies are given in Table 4. In addition to the zero-point energies, a classical desorption energy, E_c, is necessary to calculate the difference in energy between the zero-point of the surface molecule and the zero-point of the transition state, E_0. The classical desorption energy, E_c, is assumed to be identical for all of the isotopomers. The value of E_c is tuned until the slope of the Arrhenius plot obtained from the transition state model matches the slope of the observed H_2O desorption rates.

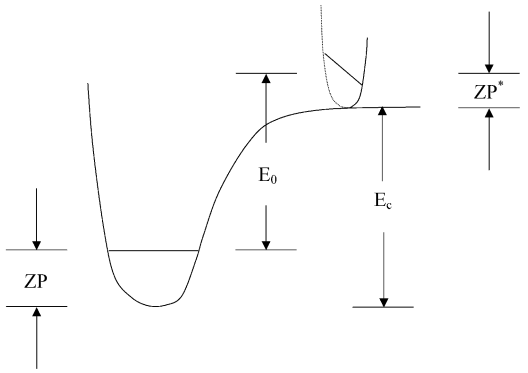

Figure 7. Energy diagram for the desorption of H_2O isotopomers from ice multilayers. E_c is the classical energy of desorption. ZP and ZP* are the zero-point energies of the surface bound molecule and transition state. E_0 is the actual desorption energy calculated from E_c, ZP, and ZP*. E_c is a free parameter that is tuned to achieve agreement between the theoretical and experimental desorption rates for H_2O multilayers.

TABLE 5: Calculated Activation Energies and Partition Functions for $T = 185$ K (Energies are in units of kcal mol^{-1}.)

	H_2O	$H_2{}^{18}O$	D_2O
E_0	13.06	13.12	13.59
q_t*	1100.	1222.	1223.
q_t	2.056	2.201	2.145
q_r*	21.08	21.26	55.49
q_r	1.011	1.011	1.041

B. Results of the Transition State Model. Table 5 lists some of the results of the transition state calculation. The difference in energy between the zero-points of the surface molecule and transition state are given for each isotopomer. The rotational and translational components of the partition functions are shown for a temperature of 185 K. The large change in rotational and translational partition functions in going from the surface bound molecule to the transition state is responsible for the large desorption preexponential that has been observed in these systems.

The transition state model affirms the isotope effect on desorption kinetics. Figure 8 shows both the observed desorption kinetics and the desorption kinetics calculated with the transition state expression. The 2-D area for the transition state and the classical desorption energy were tuned to match the observed H_2O kinetics. This tuning yielded $A = 100.6$ Å and $E_c = 16.26$ kcal mol^{-1}. The desorption kinetics for $H_2{}^{18}O$ and D_2O were then calculated by substituting the appropriate molecular mass, frequencies, and rotational constants into the tuned H_2O model. In agreement with the observations, the $H_2{}^{18}O$ ice has a slightly slower predicted desorption rate than H_2O ice. The D_2O ice has a distinctly slower predicted desorption rate than H_2O ice. The model is not quite quantitative for predicting the differences between H_2O and D_2O. However, the transition state model does qualitatively reproduce the observed isotope effect.

The small discrepancy between the observed D_2O desorption kinetics and the transition state model could arise from a number of factors. The vibrational frequencies used for the surface bound

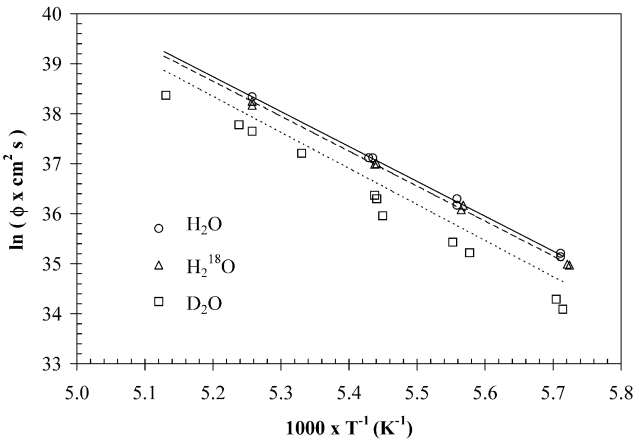

Figure 8. Arrhenius plot of the experimental desorption rates and the theoretical desorption rates. The theoretical predictions are represented by lines.

molecule are only *estimates* for the actual vibrational frequencies. The work presented here does not include the temperature dependence of the actual frequencies. For example, the frequency of the translational peak for H_2O ice is 229.2 cm^{-1} at 100 K and 222 cm^{-1} at 168 K.[49] Small shifts in frequency affect the zero-point energy of the surface bound molecules and produce a large effect on the desorption rate. The mean field approximation used here for the surface bound molecule may also contribute to the discrepancy. Each individual molecule lies in a local field that differs appreciably depending on its particular coordination to the surface.[46,47]

The transition state model has many inputs. Most of the inputs are molecular constants that have been measured or estimated and are listed in Tables 3 and 4. Two inputs were tuned to obtain agreement between the observed desorption kinetics for H_2O ice and the theoretical desorption kinetics. These inputs are the classical well depth, $E_c = 16.26$ kcal mol^{-1}, and the 2-D area of the translational portion of the transition state, $A = 100.6$ Å^2. If the transition state lies at a distance of z from the ice surface, the area of this 2-D translational box for the transition state should be $\sim\pi z^2$. The transition state is ~6 Å from the ice surface using this relationship between distance and area. Even though A was chosen to tune the model to agree with experimental data, 100 Å^2 is consistent with a transition state that is positioned only molecular dimensions from the ice surface.

C. Variational Transition State Model. A variational transition state model may improve the agreement between experiment and theory. The variational method can be more accurate for describing loose transition states that arise from potential energy surfaces without a saddlepoint. In the variational method, the transition state rate constant is calculated everywhere on the potential energy surface. The position where the calculated rate is slowest is the bottleneck in the desorption process and the best location for the transition state.

Calculation of a variational transition state rate constant on a quantitative potential energy surface is beyond our capabilities. An attempt was made to create a representative potential and calculate the variational transition state rate constant. The frequencies of a desorbing molecule were assumed to be correlated with the degree of gas-phase character of the desorbing molecule. The gas-phase character, f, was defined as the ratio of the classical potential energy of the molecule above the well bottom, E, divided by the classical well depth, E_c. A surface bound molecule at the bottom of the classical well would have zero classical potential energy and a gas-phase character of zero. A free gas-phase molecule would have classical potential energy of E_c and a gas-phase character of unity. The frequencies of a molecule with an energy between that of a surface bound molecule and a gas-phase molecule would have frequencies between those of a surface bound molecule and a gas-phase molecule.

For the variational calculation of H_2O ice, the frequencies of desorbing molecules were assumed to vary linearly with the gas-phase character, and these frequencies were interpolated from the surface bound frequency to the gas-phase frequency. A gas-phase frequency of zero was used for free translation and rotation. The eight degrees of freedom remaining after the removal of the desorption coordinate were treated as quantum harmonic oscillators. The classical well depth was assumed to be the same as the tuned transition state model, $E_c = 16.26$ kcal mol^{-1}. Subsequently, the variational transition state rate constant was calculated for gas-phase characters between zero and unity. The slowest rate constant was obtained for a gas-phase character of ~0.9. The classical well depth was then retuned and the variational treatment was repeated until a match was achieved between the variational transition state rate constant and the experimental desorption kinetics for H_2O ice at 183 K.

This iteration of the variational transition state rate constant was repeated for different frequency interpolation functions. Frequencies that varied with the square root of the gas-phase character produced the best agreement with the observed kinetics. However, the model was relatively insensitive to the functional form of the frequency variation. The tuned variational transition state model with the square root frequency interpolation was then used to calculate the theoretical desorption rates for $H_2{}^{18}O$ ice and D_2O ice.

The variational transition state calculation slightly improved the agreement between the theoretical desorption rates and the observed rates. Unfortunately, the variational transition state calculation produced a flawed transition state. A transition state with a gas-phase character of 0.9 has a classical energy 1.7 kcal mol^{-1} less than the classical energy of the free gas molecule. Transition state theory assumes that the transition state molecules cross the transition state with the average velocity of a Boltzman distribution. This average velocity corresponds to 0.5 kcal mol^{-1} of kinetic energy. Therefore, most of these variational transition state molecules do not have sufficient kinetic energy to escape from the ice surface.

V. Conclusions

The isothermal desorption kinetics of H_2O, $H_2{}^{18}O$, and D_2O ice multilayers were measured using optical interferometry for temperatures between 175 and 195 K. The desorption kinetics of H_2O and $H_2{}^{18}O$ were very similar. The desorption kinetic parameters for H_2O were $E = 13.9 \pm 0.2$ kcal mol^{-1} and $\nu = 10^{32.6\pm0.3}$ molecules cm^{-2} s^{-1} and those for $H_2{}^{18}O$ were $E_{18} = 13.8 \pm 0.2$ kcal mol^{-1} and $\nu_{18} = 10^{32.4\pm0.3}$ molecules cm^{-2} s^{-1}. $H_2{}^{18}O$ had a desorption rate that was ~9% slower than the H_2O desorption rate over the temperature range of study. In contrast, D_2O exhibited a distinctly different desorption rate that was 49−62% slower than the H_2O desorption rate. D_2O displayed both a larger desorption activation energy and larger desorption preexponential than H_2O or $H_2{}^{18}O$. The desorption kinetic parameters for D_2O were $E_D = 14.8 \pm 0.4$ kcal mol^{-1} and $\nu_D = 10^{33.4\pm0.5}$ molecules cm^{-2} s^{-1}.

The observed desorption kinetics for all the isotopomers were justified using transition state theory. The observed enhancement in the desorption preexponential was justified by the large ratio

of the partition function for a loose transition state to the partition function of a localized surface molecule. In addition, the model distinguishes D_2O as having larger moments of inertia than H_2O and $H_2{}^{18}O$. These larger moments of inertia result in lower frequencies of hindered rotation on the ice surface. On the ice surface, these lower frequencies for D_2O result in less zero-point energy and a larger desorption activation energy. At the transition state, the larger moments of inertia of D_2O result in a larger rotational partition function and a larger desorption preexponential.

Acknowledgment. The authors acknowledge the support of the National Science Foundation under Grant CHE-9905812. In addition, the authors acknowledge helpful discussions with Professor J. T. Hynes, Dr. Roberto Bianco, Dr. Akihiro Morita, and Dr. Ward Thompson from the Department of Chemistry and Biochemistry at the University of Colorado.

References and Notes

(1) Wahl, M. H.; Urey, H. C. *J. Chem. Phys.* **1935**, *3*, 411.
(2) Riesenfeld, E.; Chang, T. *Z. Phyz. Chem.* **1936**, *33*, 127.
(3) Merlivat, L.; Nief, G. *Tellus* **1967**, *19*, 122.
(4) O'Neil, J. R. *J. Phys. Chem.* **1968**, *72*, 3683.
(5) Majoube, M. *J. Chim. Phys.* **1971**, *68*, 1423.
(6) Majoube, M. *J. Chim. Phys.* **1971**, *68*, 625.
(7) Riesenfeld, E.; Chang, T. *Z. Phyz. Chem.* **1936**, *33*, 120.
(8) Szapiro, S.; Steckel, F. *Trans. Faraday Soc.* **1967**, *63*, 883.
(9) van Hook, W. A. *J. Phys. Chem.* **1968**, *72*, 1234.
(10) Matsuo, S.; Matsubaya, O. *Nature (London)* **1969**, *221*, 463.
(11) Jancso, G.; Pupezin, J.; van Hook, W. A. *Nature (London)* **1970**, *225*, 723.
(12) Jakli, G.; van Hook, W. A. *J. Chem. Eng. Data* **1981**, *26*, 243.
(13) Heras, J. M.; Asensio, M. C.; Estiu, G.; Viscido, L. *Chem. Scr.* **1984**, *23*, 245.
(14) Matsunaga, N.; Nagashima, A. *Int. J. Thermophys.* **1987**, *8*, 681.
(15) Marko, L.; Jakli, G.; Jancso, G. *J. Chem. Thermodynamics* **1989**, *21*, 437.
(16) Marti, J.; Mauersberger, K. *Geophys. Res. Lett.* **1993**, *20*, 363.
(17) Dansgaard, W. *Tellus* **1964**, *16*, 436.
(18) Alley, R. *The Two-Mile Time Machine*; Princeton University Press: Princeton, 2000.
(19) Brown, D. E.; George, S. M. *J. Phys. Chem.* **1996**, *100*, 15460.
(20) Livingston, F. E.; Whipple, G. C.; George, S. M. *J. Phys. Chem. B* **1997**, *101*, 6127.
(21) George, S. M.; Livingston, F. E. *Surf. Rev. Lett.* **1997**, *4*, 771.
(22) Livingston, F. E.; Whipple, G. C.; George, S. M. *J. Chem. Phys.* **1998**, *108*, 2197.
(23) Livingston, F. E.; George, S. M. *Defect Diffus. Forum* **1998**, *161*, 25.
(24) Livingston, F. E.; George, S. M. *J. Phys. Chem. B* **1999**, *103*, 4366.
(25) Davy, J.; Somorjai, G. *J. Chem. Phys.* **1971**, *55*, 3624.
(26) Haynes, D. R.; Tro, N. J.; George, S. M. *J. Phys. Chem.* **1992**, *96*, 8502.
(27) Brown, D. E.; George, S. M.; Huang, C.; Wong, E. K. L.; Rider, K. B.; Smith, R. S.; Kay, B. D. *J. Phys. Chem.* **1996**, *100*, 4988.
(28) Speedy, R. J.; Debenedetti, P. G.; Smith, R. S.; Huang, C.; Kay, B. D. *J. Chem. Phys.* **1996**, *105*, 240.
(29) Livingston, F. E.; George, S. M. *J. Phys. Chem. A* **1998**, *102*, 10280.
(30) Mak, C. H.; Brand, J. L.; Deckert, A. A.; George, S. M. *J. Chem. Phys.* **1986**, *85*, 1676.
(31) Thiel, P. A.; Madey, T. E. *Surf. Sci. Rep.* **1987**, *7*, 211.
(32) George, S. M. *J. Vac. Sci. Technol. A* **1986**, *4*, 2394.
(33) Livingston, F. E.; Smith, J. A.; George, S. M. *Surf. Sci.* **1999**, *423*, 145.
(34) Rottger, K.; Endriss, A.; Ihringer, J.; Doyle, S.; Kuhs, W. F. *Acta Crystallogr. Sect. B: Struct. Sci.* **1994**, *50*, 644.
(35) Warren, S. G. *Appl. Opt.* **1984**, *23*, 1206.
(36) Berland, B. S.; Brown, D. E.; Tolbert, M. A.; George, S. M. *Geophys. Res. Lett.* **1995**, *22*, 3493.
(37) Redondo, A.; Zeiri, Y.; Low, J.; Goddard, W. I. *J. Chem. Phys.* **1983**, *79*, 6410.
(38) Kroes, G. *Surf. Sci.* **1992**, *275*, 365.
(39) Devlin, J. P.; Buch, V. *J. Phys. Chem.* **1995**, *99*, 16534.
(40) Bolton, K.; Petterson, J. B. C. *J. Phys. Chem. B* **2000**, *104*, 1590.
(41) Benedict, W. S.; Gailar, N.; Plyler, E. K. *J. Chem. Phys.* **1956**, *24*, 1139.
(42) Fraley, P. E.; Rao, K. N.; Jones, L. H. *J. Mol. Spectrosc.* **1969**, *29*, 312.
(43) Fraley, P. E.; Rao, K. N. *J. Mol. Spectrosc.* **1969**, *29*, 348.
(44) Williamson, J. G.; Rao, K. N.; Jones, L. H. *J. Mol. Spectrosc.* **1971**, *40*, 372.
(45) Kyro, E. *J. Mol. Spectrosc.* **1981**, *88*, 167.
(46) Delzeit, L.; Devlin, J. P.; Buch, V. *J. Chem. Phys.* **1997**, *107*, 3726.
(47) Hernandez, J.; Uras, N.; Devlin, J. P. *J. Chem. Phys.* **1998**, *108*, 4525.
(48) Bertie, J. E.; Whalley, E. *J. Chem. Phys.* **1964**, *40*, 1637.
(49) Bertie, J. E.; Whalley, E. *J. Chem. Phys.* **1967**, *46*, 1271.